

Aperiodic flow-induced oscillations of collapsible tubes: a critical reappraisal

C.D. Bertram^{a,*}, J. Timmer^b, T.G. Müller^b, T. Maiwald^b, M. Winterhalder^b,
H.U. Voss^b

^a Graduate School of Biomedical Engineering, University of New South Wales, Sydney, NSW 2052, Australia

^b Freiburger Zentrum für Datenanalyse und Modellbildung, Fakultät für Physik, Albert-Ludwigs-Universität Freiburg, Eckerstraße 1, 79 104 Freiburg, Germany

Received 7 April 2003; received in revised form 14 October 2003; accepted 21 November 2003

Abstract

The evidence for the aperiodic self-excited oscillations of flow-conveying collapsible tubes being mathematically chaotic is re-examined. Many cases which powerfully suggest nonlinear deterministic behaviour have not been recorded over time-spans which allow their exhaustive examination. The present investigation centred on a previously recorded robust and generic oscillation, but more recent and more discerning tests were applied. Despite hints that a low embedding dimension might suffice, the data appeared on most indices high-dimensional. A U-shaped return map was found and modelled using both radial basis functions and polynomials, but lack of detailed structure in the map prevented effective parameter estimation. On the basis of power-law rather than exponential divergence of nearby trajectories, and of inability to discriminate against behaviour which would also be manifested by a surrogate consisting of a noise-perturbed nonlinear periodic oscillator, it is concluded that the data do not support the idea that the aperiodicity in the particular oscillation examined is caused by deterministic chaos. There was evidence that the distributed nature of the physical system might underlie aspects of the high dimensionality. We advocate equally searching testing of any future candidate chaotic oscillations in the investigation of collapsed-tube flows.

© 2003 IPEM. Published by Elsevier Ltd. All rights reserved.

Keywords: Nonlinear dynamics; Deterministic chaos; Time-series analysis; Self-excited oscillation

1. Introduction

Fluids are transported in the mammalian body through conduits which, having flexible walls, are potentially collapsible. The study of collapsible tubes is motivated partly by the desire to understand the properties of these biological conduits, but also by the intriguing nature of the physical system per se. Investigation readily shows that when the conduit is collapsed by external pressure, and there is a through-flow at substantial Reynolds number (a few hundred or more), self-excited or flow-induced oscillation can occur.

Nonlinear dynamics allows us to understand how low-dimensional deterministic models give rise to

complex, apparently stochastic, behaviour [1]. In high-Reynolds-number experiments on aqueous flow through rather thick-walled collapsible tubes, Bertram et al. [2] observed both periodic and aperiodic self-excited oscillations. On the evidence of the relation between transmural pressure and tube cross-sectional area, the system is highly nonlinear, and as a distributed fluid-dynamic system it is dissipative and has an infinite number of degrees of freedom. Dynamical chaos requires nonlinearity and a minimum of three degrees of freedom; dissipation tends to simplify the topological structure of trajectories in phase space, allowing an infinite-dimensional system to exhibit finite-dimensional behaviour [3]. The circumstances are thus sufficient for the appearance of low-dimensional chaos. Furthering this expectation is the richness of variety of oscillation modes of which the system is known to be capable; Bertram et al. [2] showed 11

* Corresponding author. Tel.: +61-2-9385-3928; fax: +61-2-9663-2108.

E-mail address: c.bertram@unsw.edu.au (C.D. Bertram).

qualitatively distinct waveforms, many aperiodic, while in a thinner tube of similar material, Bertram and Elliott [4] distinguished 19 periodic waveforms.

Bertram et al. [2] applied then-available dynamical systems methods to the analysis of the aperiodic oscillations. They mapped their observations into a two-dimensional control space, corresponding to the control of the experiment through adjustment of the flow-driving head or upstream pressure p_u and the pressure applied external to the flexible conduit, p_e . However, it was found that replacement of p_e with the dependent variable $\bar{p}_{e2} = p_e - \bar{p}_2$, where p_2 = pressure at the tube exit and \bar{p} is the time-average of p , allowed divergent instabilities to be mapped as disallowed zones in control space. This use of a dependent variable departed from usual dynamical systems practice. Bertram et al. [2] showed amplitude/frequency spectra, phase-plane portraits of pairs of their recorded time-variables (p_1 , p_2 , Q_2 and A , where p_1 = pressure at the tube entrance, Q_2 = volume outflow-rate and A = tube area at the ‘throat’, the site of maximal oscillatory activity), and time-delay phase-plane portraits. Sectioning the trajectories so formed, they derived first-return maps, demonstrating that some of the aperiodic oscillations had the character of a noisy amplitude-modulated waveform. In the case of one aperiodic mode, it was demonstrated by overlaying sections that there was approximate repetition of a complex cycle which on the basis of its autocorrelation function appeared to be a period-8 oscillation.

Singular value analysis [5] was used to demonstrate that another aperiodic mode had the main structure of a 2-torus, with a further small-amplitude higher-frequency oscillation superimposed at one consistent phase (maximal collapse at the tube throat). After reconstruction from the principal components of the singular spectrum, and in places where the data density allowed, local dimension was estimated by the method of Broomhead et al. [6]. The estimates ranged between two and five [2], although problems of data sparsity prevented conclusive results.

Qualitative bifurcation topologies were evolved to explain the main features of the oscillatory dynamics as exposed in the modified-control-space mappings. The most promising candidate topology combined a pair of fold bifurcations (explaining the observed hysteresis and divergence) with a supercritical Hopf and a homoclinic connection (explaining the gradual onset and abrupt disappearance of oscillation with p_e -reduction)—see Thompson and Stewart [3] for further explanation of these terms. However, despite these successes of dynamical system methodology, Bertram et al. [2] concluded that deterministic chaos had not been proven to underlie the observed aperiodic oscillations.

Nevertheless, Jensen [7], who investigated a one-dimensional model of a collapsible tube, found encour-

aging signs that the system might indeed be chaotic. His model, based on that of Cancelli and Pedley [8], proved to contain overlapping regions of (\bar{Q}, \bar{p}_{e2}) -control space where a given mode of oscillation was unstable, constituting the first theoretical evidence corresponding to the multiple modes that Bertram et al. [2] had observed. At (\bar{Q}, \bar{p}_{e2}) -coordinates where more than one mode was simultaneously unstable, he computed oscillations suggestively similar to the observed amplitude-modulated aperiodic modes, and also an oscillation that was aperiodic by intermittent switching between waveform morphologies. However, he did not apply exhaustive tests for the existence of chaos.

Further analysis of the observed aperiodic oscillations was conducted by Bertram and Tian [9] and by Bertram [10]. The largest Lyapunov exponent was approximated by the method of Wolf et al. [11] and shown to be significantly positive. Since the data were regarded as possibly emanating from a chaotic attractor with added noise, a method based on singular value analysis and cross-correlation of two parallel computations of local trajectory divergence was devised which yielded a ‘degree of chaos’ index. This could be extrapolated to the situation of zero noise. The 1995 paper [10] reviewed further dynamical system methods which had been applied to the data. These included searching for close returns to the same local neighbourhood on contiguous ‘orbits’, both graphically and numerically, on the basis that unstable periodic orbits organise the aperiodic flow on a chaotic attractor [12]. However, these further data analyses did not resolve the question of whether low-dimensional chaos caused the observed aperiodicity.

In a different approach, Armitstead et al. [13] used continuation software [14] to map the loci in two-dimensional parameter space (p_u , p_e) of bifurcations in the dynamical behaviour of a lumped-parameter model of flow in a collapsed tube. The model [15], while extremely crude, had predicted realistic-looking self-excited oscillations and demonstrated their dependence on the extent of downstream resistance and inertia. Armitstead et al. [13] showed that the model, although of third order, was confined to a two-dimensional central manifold by an eigenvalue that always remained real and negative. Thus repetitive limit-cycle oscillations were all that could be expected; chaos was not possible, at least in the parameter regime examined.

In yet another approach, the question was posed: what happens if forcing oscillations are imposed from upstream on a collapsible tube executing repetitive self-excited oscillation? A servo-controlled hydraulic actuator was used to power a piston pump providing a pulsatile addition to the previously steady upstream head, while the tube remained at an operating point in parameter space that otherwise yielded periodic

oscillation. Predominantly, entrainment of the tube by the forcing led to complex long-period cycles representing ‘mode-locking’, i.e. a fit between several cycles of the forcing and a different number of cycles of the tube oscillation [16]. However, extensive aperiodic oscillation was also encountered, and this was shown by fractal dimension and other standard tests to result from the action of a low-dimensional chaotic attractor [17].

This experimental finding paralleled the result of adding analogous upstream forcing to the lumped-parameter model, in the process converting it to a fourth-order system. With the almost unlimited resolution available numerically, the classic signs of a chaotic system could be obtained, including a period-doubling cascade leading to aperiodicity, and a toroidal oscillation topology which in Poincaré section had fractal structure [18].

The clear evidence of chaos in the forced system, both the numerical one and the experimental, and the lack of capability for same in the unforced model, reinforced doubt that the aperiodic oscillations from the unforced experiment could be ascribed to this explanation. In this paper, we reopen the question of what caused these aperiodic oscillations, using now tools of nonlinear dynamics which were not available at the time of the earlier analyses.

2. Methods

Our collapsible-tube experiment has been fully documented in published papers referred to in the Introduction, particularly that by Bertram et al. [2], so only the briefest of descriptions will be given here. The tube was of silicone rubber (Dow Corning Silastic[®]), of nominal inside diameter 12.7 mm and wall thickness 2.4 mm. Tubes of four different lengths were investigated, but that in use when the data to be analysed here were recorded was 17.4 diameters long once suspended (in air) with slight longitudinal tension between the rigid pipe connections to the recirculating-flow system. The fluid within was basically water, with minor admixtures of ionic solutes providing conductivity for area measurement by conductance catheter (not used here), and buffering for corrosion resistance in the recirculating flow tanks. Operating points in a range up to 200 kPa of driving head p_u and 0.5 l/s of flow-rate Q were investigated using a constant-pressure source. The observed behaviour at the operating point is also affected by the passive hydrodynamic properties (resistance to flow, fluid inertia, etc.) of the apparatus upstream and downstream of the tube, particularly downstream; oscillation is inhibited by excess downstream resistance, and the natural frequency varies inversely with downstream inertia. Upstream inertia (between the delivery

point of the flow-driving constant head and the tube entrance) determines the extent to which the tube is perfused at constant pressure. The downstream resistance here corresponded to that labelled R'_2 in Bertram et al. [2], wherein full details of the lumped properties of the apparatus were given; the distributed (frequency-dependent) properties of the apparatus were measured by Bertram and Butcher [19]. Recordings were made using a 12-bit a/d converter at 500 Hz; this rate sufficed to avoid aliasing in the oscillatory content of the pressure signals, and comfortably exceeded the 100 Hz bandwidth of the electromagnetic flowmeter signals (set by the internal demodulation filter). The pressure-transducing systems measuring p_1 , p_2 and p_e were all carefully calibrated to 20 kPa/V, thus allowing us to monitor by real-time voltage subtraction during the experiment the difference signal representing $p_{e2} = p_e - p_2$, of which the low-pass-filtered time-average component was used as one of the experimental control parameters to set the operating point. Similarly, the two channels of electromagnetic flowmeter signal were set to the same calibration as each other, a sensitivity that was chosen to allow all operating points in the range that could be reached to be recorded in a ± 10 V a/d converter input range without recalibration. These choices of experimental procedure meant that the upstream signals p_1 and Q_1 , which varied less than their downstream counterparts p_2 and Q_2 when the operating point was oscillatory, covered only a fraction of the whole 12-bit a/d converter range.

At the time when the aperiodic oscillations were first observed, our recording equipment was not capable of acquiring long continuous stretches of data at a high sample rate, as was needed in order to fill a potentially high-dimensional embedding space with trajectories even in rarely visited locations. This need was in due course met, but some of the most intriguing waveform morphologies captured in all-too-brief recordings earlier could not be found again. In this paper, we concentrate on a particular aperiodic waveform morphology which appeared robust enough that multiple long recordings could be made of it. Known to us as lg9, 32,700 samples of the data were recorded at an operating point defined by $p_u = 171$ kPa, $p_e = 173.5$ kPa, yielding $\bar{p}_{e2} = 134$ kPa, $\bar{Q} = 227$ ml/s. The Reynolds number based on tube diameter was about 23,000. A window of the lg9 p_2 -data formed Fig. 7 of Bertram [10], and Fig. 7c of Bertram et al. [2] showed a waveform of approximately the same morphology. Our software was set up for recording six channels simultaneously; of these three were devoted to monitoring variables needed to assure us of stationarity, so the oscillation was registered by means of the time-variables p_1 , p_2 and Q_1 . In another dataset of equal length (lg8), Q_2 was also recorded; a window of these

data is illustrated in Fig. 1. The lg8 dataset is available for downloading at <http://www.gsbme.unsw.edu.au/download.htm>.

3. Analysis

3.1. Software

The nonlinear analyses of the previous papers on the aperiodic collapsible-tube data were performed using software written for the purpose. In the interim, software packages have become available which perform most of the standard tests. The package utilised here was Tisean (Time Series Analysis) v2.1 by Hegger et al. [20]. Thorough documentation is provided at the website (http://www.mpipks-dresden.mpg.de/~tisean/TISEAN_2.1), but additional background material is given by Kantz and Schreiber [21]. Other routines were written in Matlab, C, IDL and Fortran. Details of the function of each test are given in the rest of this section.

3.2. Waveforms

For dynamical-system purposes, a first step is to normalise time series to zero mean and unit standard deviation, so the units of the original signal are irrelevant. For this reason the traces in Fig. 1 are presented in a/d-converter integers. The calibrated ranges were 142.8

to 187.1 kPa for p_1 and -77.5 to 147.7 kPa for p_2 (relative to atmospheric pressure at the downstream exit to the recirculating-system collecting tank); Q_1 varied between 202 and 261 ml/s. As can be seen in the figure, the recorded signals for p_1 , p_2 , Q_1 and Q_2 varied over approximately 450, 2300, 125 and 550 integers, respectively, the proportions 450:2300 (0.20) and 125:550 (0.23) being true measures of the upstream-to-downstream relative peak-to-peak variation of the pressures and flow-rates, respectively. We conclude that Q_1 in particular, while apparently smoothly delineated in Fig. 1, is subject to a discretization artefact. The flow-rate signals show predominantly two components: a large-amplitude oscillation and a smaller, higher-frequency oscillation. The period of this faster component occupies about ten data points; thus its orbital trajectories in phase space will be polygonal rather than smoothly curved, unless the data are interpolated. In the pressure signals, the same two dominant components are seen, although the higher bandwidth is manifested in sharper peaks and troughs. The downstream pressure also exhibits a third component, a small-amplitude high-frequency transient occurring at the time of waveform troughs; this is caused by flutter between the opposite walls of the tube at the throat at the instant of maximal collapse. This third component represents an additional complexity from the point of view of dynamical systems analysis. Thus, of the signals p_1 , p_2 and Q_1 available in lg9, we regarded p_1 as

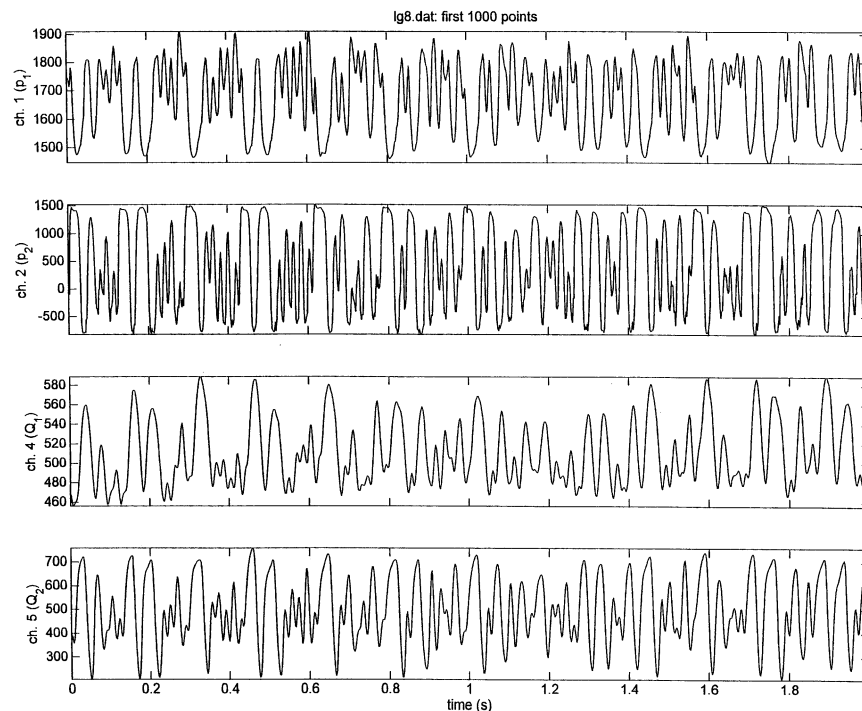


Fig. 1. The first 1000 data points (out of 32,700) for each channel in the file lg8. The channels are, from the top, upstream pressure (p_1), downstream pressure (p_2), upstream flow-rate (Q_1) and downstream flow-rate (Q_2), all in a.d.c. integers.

the best candidate for detailed examination. However, some of the outcomes could be established without difficulty on the Q_1 signal, and in some cases tests on all three signals yielded informative comparisons.

3.3. Nonlinearity and stationarity

A fundamental test is whether the system from which the signals emanate is nonlinear. An objective and non-trivial test can be mounted by comparing the data with suitable surrogates. The surrogates are realizations of the null hypothesis that the data were generated by a constrained linear random process, where the constraints force the surrogates to share certain properties with the data. Fourier-based surrogates share the amplitude spectrum of the original data, but have randomised phase. It is then desirable to constrain the surrogates further, to have the same distribution of values as the data. This two-step approach is realized iteratively in the algorithm used [22].

A basic requirement of the data is that they emanate from a stationary system; nonstationarity would cause the system erroneously to appear high-dimensional even if it were not. This property can be examined in a recurrence plot, consisting of the time-index coordinates (i, j) of pairs of points whose delay vectors are separated by ε or less.

3.4. Portraits

For all the sophistication and complexity of mathematical tools for the analysis of nonlinear data, inspection of the trajectories in phase space remains among the most powerful techniques. Much effort was devoted to creating Poincaré sections of the data, in an attempt to find structure that could be the subject of a critical test of any parametric or nonparametric modelling endeavours. A fundamental theorem of nonlinear dynamics [23] states that structure revealed by a judicious embedding and sectioning is a characteristic signature of the data, no matter how many other sections fail to show it.

The optimal delay for embedding purposes is usually thought to be that delay at which the mutual information [24] has its first minimum. However, mutual information, which should be preferred for complex attractors such as the bi-lobar Lorenz, involves density estimation and, therefore, depends on parameters which have to be chosen optimally according to the system under investigation. For simpler oscillating systems such as the Rössler or the van der Pol, optimal delay is more reliably assessed using the autocorrelation function. Although the oscillations here present both larger, slower and smaller, faster cycles, the overall pattern is predominantly comparable with the aperi-

odic limit cycles of the velocity-forced van der Pol system [9].

The Tisean routine for creating Poincaré sections only dealt with time-delay embedding of a single data set. In view of the fact that three channels of data were available for lg9 and four for lg8, two-dimensional Poincaré sections could be created from three-dimensional data sets. This also allowed sections and return maps to be created of data after projection along the first three principal components, using Tisean to perform the principal-component analysis.

We also applied nonlinear filtering to the experimental return map. A simple algorithm from Tisean was initially used, which takes a locally constant approximation to the dynamics and replaces the centre point. However testing on noise-corrupted versions of the logistic map revealed that this algorithm worked unevenly, being much more effective where the section being filtered was aligned with the axes than where it was diagonally inclined. Consequently, Tisean's more sophisticated locally projective algorithm [25], which worked satisfactorily on our test data, was used instead.

3.5. Dimensions

Theoretically, the minimum proper embedding dimension m for an attractor lying in a smooth D -dimensional manifold is $m = 2D+1$ [23]. However, fewer dimensions may suffice for particular manifolds [26], and D is usually not known. Alternative methods are therefore needed to estimate m . The method of false nearest neighbours [27] posits that an adequate choice of m will result in only true neighbours in attractor space being neighbours in embedding space, and that after mapping according to the smooth dynamics, the neighbours will still be neighbours, in a neighbourhood distorted according to the Lyapunov exponents. Too small a choice of m will give false neighbours which will map to quite different regions of the attractor.

Another approach to the question of an adequate embedding space is found in the concept of singular-value decomposition, whereby the principal-component vectors are calculated from the eigenvalues of the covariance matrix formed from the data [5]. The data are then reconstructed in principal-component space, using just that number of vectors needed to reach the cumulative variance of the original data.

The most widely accepted way to estimate attractor dimension is the method of Grassberger and Procaccia [28], in which the correlation integral $C(\varepsilon)$ is computed for a variable range of neighbourhood size ε . The slope of this plot, if constant over an adequate range of ε , indicates the (noninteger) correlation dimension d_2 .

3.6. Unstable periodic orbits

Unstable periodic orbits are considered an organising principle of chaotic attractors, which approach them arbitrarily closely (the closer, the longer) before diverging back to normal chaotic trajectories. However, while unstable periodic orbits are fundamental to dynamical theory, it is not clear that they are robust to even small amounts of noise. Bertram [10] used a close-return method (D.P. Lathrop, personal communication) to identify the relative frequency of occurrence of approximately closed orbits of varying lengths in the lg9 data. Tisean's routine for finding unstable periodic orbits works on a model of the data, not the data themselves, and it was found difficult to relate the reported orbits to the lg9 data. Instead we applied the Lathrop method to surrogate data generated from a stochastic differential equation (SDE), representing noise applied to the acceleration term of the otherwise-periodic Van der Pol oscillator.

3.7. Lyapunov exponents

Bertram and Tian [9] computed significantly positive values of the largest Lyapunov exponent λ_1 , indicating exponential divergence of initially close starting points, one of the characteristic behaviours of a chaotic system. However, the algorithm used then [11] assumed that any divergence was exponential, and did not test this assumption. Today the question is examined graphically, plotting semi-logarithmically an index $S(\varepsilon, m, t)$ of the separation against time t (in units of samples), ε being the initial neighbourhood size. Quoting from Tisean documentation, "If S exhibits a linear increase with identical slope for all m larger than some m_0 and for a reasonable range of ε , then this slope can be taken as an estimate of the maximal exponent."

3.8. Prediction

Linear prediction of the data has been introduced already in the context of surrogates. Several further approaches to prediction were applied. The simplest and most robust method of nonlinear prediction is to approximate the dynamics locally by a constant. Quoting from the relevant Tisean documentation, the "program makes a zeroth order ansatz and estimates the one step prediction errors of the model on a multivariate time series. This is done by searching for all neighbours of the point to be forecasted and taking as its image the average of the images of the neighbours. The given forecast errors are normalized to the standard deviations of each component."

A next step in sophistication "makes a local linear ansatz and estimates the one step prediction error of the model ... as a function of the neighbourhood size".

The graph of average forecast error against neighbourhood size is Casdagli's [29] DVS-plot (deterministic vs. stochastic). Four outcomes are distinguished: the system is linear or nonlinear, and there is or is not a source of noise. From the large-neighbourhood right-hand side of the plot, one sees whether the system is linear (prediction error is independent of size) or nonlinear (prediction error increases with size, as the system curves away from the hyperplane prediction). From the small-neighbourhood left-hand side of the plot, one sees whether there is noise in the system; if there is, prediction error increases abruptly at some minimum neighbourhood size at which the noise makes the hyperplane fit inaccurate. This point moves to larger sizes as m increases because of the requirement to find an adequate number of neighbours while the noise becomes ever more sparsely distributed in m dimensions. If the system is noise-free, the hyperplane fit will work down to the same minimum neighbourhood size irrespective of m , because the data all lie on the attractor, which has its characteristic shape, independent of how many dimensions are used to embed.

4. Results

4.1. Nonlinearity and stationarity

Nineteen surrogates of the first 1536 points of the Q_1 trace, rescaled to zero mean and unit standard deviation, were created. A locally constant nonlinear predictor was then used to forecast the progress of the time series, one point ahead, on the basis of the points found in a local neighbourhood which was 10% of the time-series standard deviation in radius in a three-dimensional delay embedding. In this case the delay used was one point, which is sub-optimal (see above), but the result is not in doubt. The prediction error was found to be less for the data than for any of the surrogates, allowing rejection of the null hypothesis at the confidence level $p < 0.05$.

A recurrence plot was made of the rescaled Q_1 with $m = 2$, $d = 10$ (the plot is reasonably insensitive to the choice of m), and a neighbourhood size ε equal to 10^{-3} of the data interval. The recurrence plot is reproduced as Fig. 2, showing almost ideal stationarity. This is a belated tribute to the precautions taken to achieve accurately constant upstream head in the recirculation system [30].

4.2. Portraits

The autocorrelation and mutual information methods for finding optimum delay were applied to all three variables (Q_1 , p_1 and p_2). Applied to the above window from the Q_1 trace, the computation of the mutual

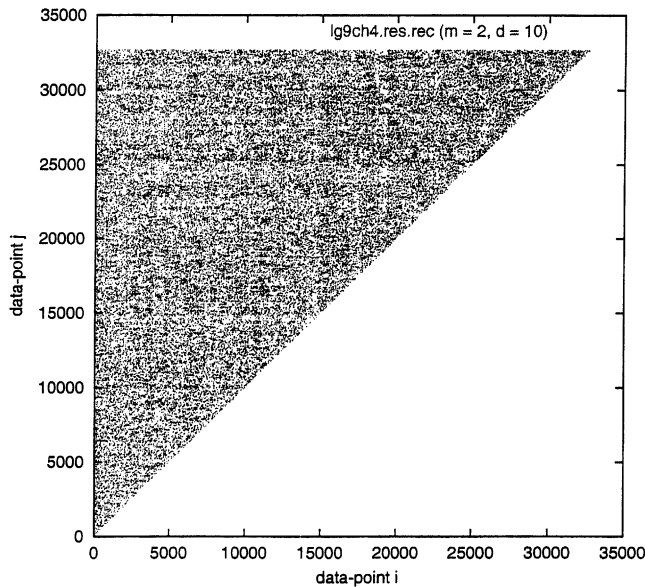


Fig. 2. The recurrence plot for Q_1 from the file lg9, with $m=2$, $d=10$ and $\varepsilon=10^{-3}$.

information (based on a simple fixed mesh of boxes) showed a shallow minimum at delay $d=17$, but decline had effectively ceased at $d=9$. Working with all 32,700 data, the first zero of the autocorrelation occurred at $d=4$ for p_1 , between $d=3$ and $d=4$ (closer to 4) for p_2 , and between $d=6$ and $d=7$ for Q_1 . For p_1 and p_2 there was a very weak local minimum of mutual information agreeing with the autocorrelation result, but not for Q_1 . With a shortest main period of the order of ten points, it is clear that $d=3$ is indeed the best result, presumably obscured by the discretization artefact in Q_1 .

Working with first-return maps of the section times, we found a clumping of the return times as shown in Fig. 3, such that returns tended to occur at multiples of a basic period about ten sample points long. Of the two largest groups in the map, both corresponding to the basic period, long times were usually followed by short times, and short times by short or long times, but seldom long by long.

By two-dimensional Poincaré sectioning we discovered a further interesting structure: a U-shaped return map, seen for instance in the (p_1, Q_1) -plane section times from the re-scaled lg9 data, sectioned at re-scaled $p_2=0$ in the rising direction, as shown in Fig. 4a. To test whether the low-dimensional dynamics thus seen could be modelled using a deterministic map, we used the method of optimal transformations [31]. This method is based on a nonparametric additive model estimation, utilising the ACE algorithm [32]. The most optimal fit to the data shown in Fig. 4a was achieved with a six-component additive model. For numerical integration of the nonparametric model esti-

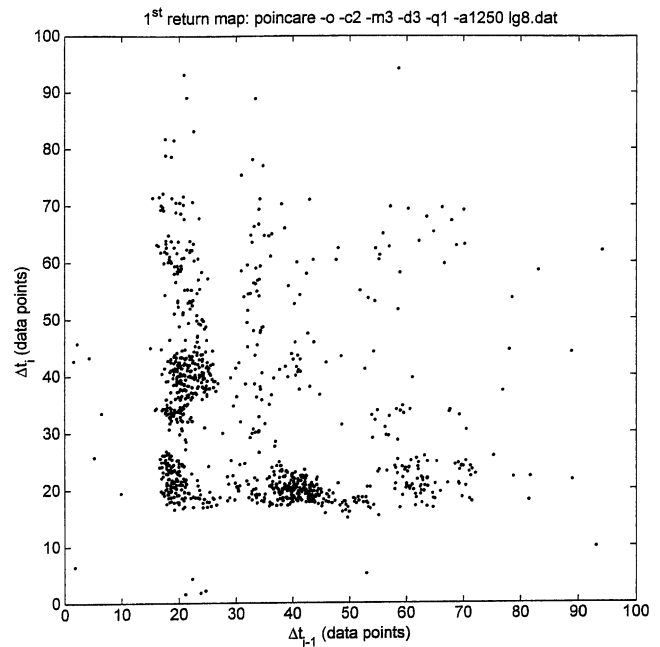


Fig. 3. First return map of a Poincaré section for p_2 from the file lg8, time-delay-embedded in three dimensions with $d=3$, sectioned normal to the first axis at data-point value 1250, showing clumping at $\Delta t=20$ and multiples thereof.

mate, sixth-order polynomials were used. As can be seen from Fig. 5, this model reproduced the main shape. Not being limited to the 1300 or so section-plane intersections of the original experimental data, the model produced a return map with much additional fractal structure.

Effort was accordingly devoted to nonlinear filtering of the experimental return map, to see whether similar structure could be discerned. Such additional structure is needed to enable one to tell whether such a model such as our polynomial one fitted the data by chance or by virtue of its similarity to the mechanism underlying the data. A locally projective algorithm gave results as shown in Fig. 4b. However, the structure so revealed did not resemble particularly closely that in the polynomial model's section. In this context it is pertinent also to remember [20] that nonlinear filtering, while adept at apparently 'cleaning-up' a noisy map, can create pseudo-structure where none exists.

4.3. Dimensions

Applying the method of false nearest neighbours to Q_1 (not re-scaled), by $m=3$ the fraction of false neighbours was already down to 0.0059, thence declining to 0.0031 at $m=4$, 0.0016 at $m=5$ and 0.0006 at $m=7$. This confirmed the well-known finding that while it works well on analytical attractors, the method does not give unambiguous answers for data which include

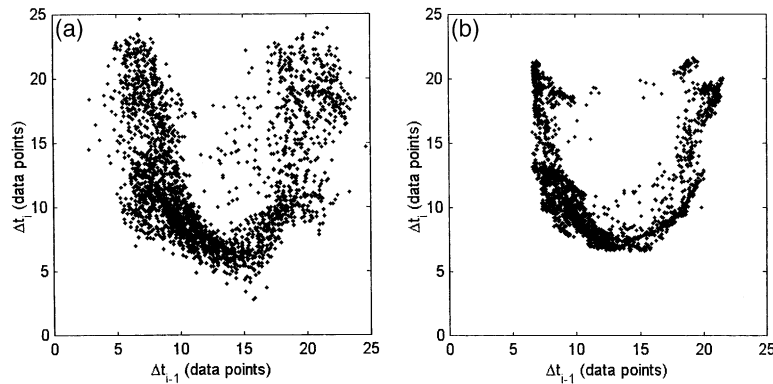


Fig. 4. The U-shaped map of first-return times achieved by a Poincaré section normal to the p_2 -axis of the re-scaled three-dimensional (p_1 , p_2 , Q_1)-plot from the file lg9. The raw data are shown in panel a; panel b shows the result of nonlinear noise reduction by three iterations of a locally projective algorithm on a two-dimensional manifold with $m=6$, using a neighbourhood radius of 0.5 and a minimum of 50 neighbours.

any noise. However, the result does suggest that $m=3$ may be adequate for noncritical uses in this case.

The principal components of the re-scaled Q_1 were found with $m=20$ and $d=1$; the cumulative variance reached essentially one using six principal components. Projections of the first 2000 points onto the (pc_1 , pc_2)-, (pc_1 , pc_3)- and (pc_2 , pc_3)-planes were also drawn, as part of the investigation of phase space and Poincaré sections.

The correlation integral was calculated for all three variables (Q_1 , p_1 and p_2) after re-scaling, with $d=3$ and 5, and $d(\log C[\varepsilon])/d(\log \varepsilon)$ was plotted against ε , for m from 1 to 10. Large fluctuations were present from one value of ε to the next for all m with Q_1 . Slightly better results were achieved using p_1 ; a still fluctuating but

reasonably constant level (which however increased with m) was achieved over one and a half decades of ε . Smoothing arithmetically the slope output over an interval of $2a+1$ points gave best results with $a=4$. Over two decades of readable result were obtained using p_2 (see Fig. 6); clearly the discretization noise in Q_1 and, to a lesser extent, p_1 , is a problem here. The correlation dimension d_2 increased with m , reaching about 4 at $m=10$. Combining 10-dimensional delay-embedding ($d=3$) and all three signals, a total embedding dimension of 30 was reached, with the d_2 plateau no longer really flat, but rather sloping from a minimum of 4 at $\varepsilon=1$ to a maximum approaching 6 at $\varepsilon=0.2$. This is not to be believed; quite aside from lack of constancy, a dimension of six would be one imposed

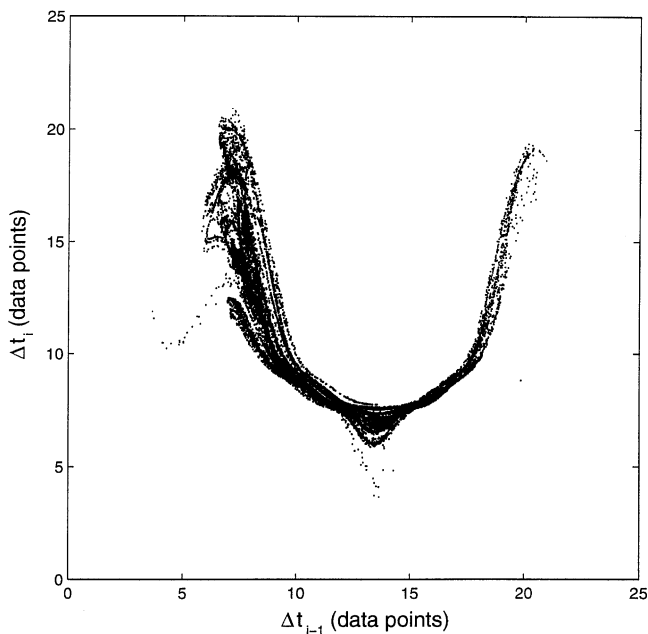


Fig. 5. The first-return map produced by the sixth-order-polynomial nonparametric model fitted to the map data shown in Fig. 4a.

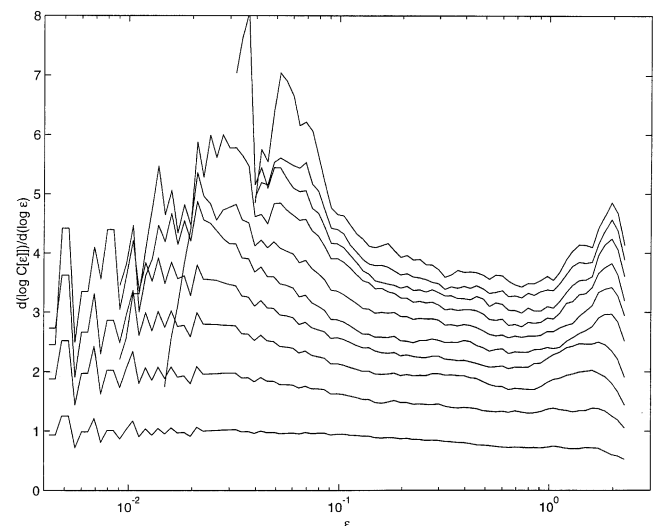


Fig. 6. The slope of the correlation integral plotted against local region size ε , with local smoothing ($a=4$). The p_2 signal from lg9 was used with 10-dimensional delay ($d=3$) embedding, giving a maximum $m=10$ and a corresponding number of curves. Successively higher values of m yield progressively greater slopes.

by the length of the data set rather than attractor dynamics.

4.4. Unstable periodic orbits

We generated two Van der Pol oscillator-space time-variables, each of 32,000 points. Applied to the time-variable representing location, with $d=5$ as indicated by autocorrelation minimum, our close-return detection scheme found instances of both the basic orbit length of around 20, and multiples of it. The ability of such nonchaotic surrogates as these to fool a close-return method indicates the necessity to examine the stability of purported unstable periodic orbits, for instance by the method of So et al. [33], which reverses the dynamics in the map vicinity of an unstable periodic orbit so as to zero in on it. These of course are methods available to the investigator of a mathematical attractor which are denied to those interested in the analysis of experimental results.

4.5. Lyapunov exponents

The algorithm of Kantz [34] was applied first to the rescaled Q_1 data of lg9 with $m=2, 3$ and 4. All the curves for values of ε up to 0.0296 and a given m coincided exactly; only that for $\varepsilon=0.0527$ differed, being always slightly higher. At $m=4$, any possibly linear slope was interrupted by regularly occurring slope discontinuities, every five samples, this being the value of d specified. At $m=3$, the effect was less, and at $m=2$, approximate linearity was present for times between three and nine samples.

The solution to the problem creating the discontinuities is to resample the data so as to keep only every d th point, then compute S with $d=1$. On this basis, the same plot was generated for p_1 of the lg9 data. Against linear time, S showed no linear portion for any of $m=3$ to 6; against log time, S was close to linear, as shown in Fig. 7. Since the definition of S incorporates a logarithm already, this is power-law behaviour. Of course, to measure the slope, if S is calculated with natural logarithms, so must one plot $\log_e t$. We found slopes in the region of one: 0.86 with $m=5$, 0.95 with $m=6$, and 0.97 with $m=7$. These slopes are *not* Lyapunov exponent estimates, being taken from log-log plots, and thus indicating non-exponential divergence of neighbouring points.

4.6. Prediction

The locally constant nonlinear predictor algorithm was applied to all three lg9 channels (p_1 , p_2 and Q_1) after re-scaling, with $d=5$ and 10. The forecast errors were in general least for Q_1 , although all the prediction errors exceeded 0.5 by forecast time equal to seven

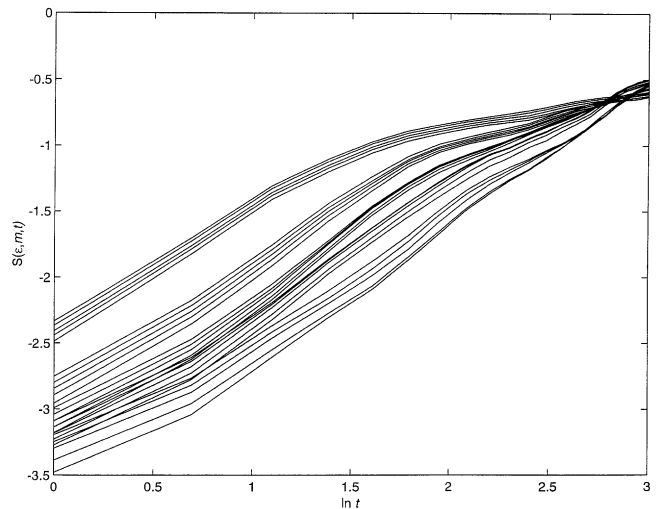


Fig. 7. The plot of S vs. $\log_e t$, for p_1 from the file lg9, showing approximately constant slope indicating power-law divergence. The top band of curves is for $m=3$; successively lower bands are for $m=4, 5, 6$ and 7. Within each band, curves are plotted for five choices of ε .

samples. The results with $d=5$ and 10 were almost identical.

The DVS procedure was also applied to the rescaled lg9 data. We produced curves of average forecast error against neighbourhood size for p_1 , p_2 and Q_1 , with $d=1, 2$ or 3 and for $m=2$ to 10; those for p_2 at $d=3$ are shown in Fig. 8. The behaviour of the pressure curves for $d=1$ at low neighbourhood sizes was intriguing: between $m=2$ (p_1) or 3 (p_2) and $m=10$, the small-neighbourhood onset of the deterministic part of the curve started at sizes ranging over less than a decade, emphasizing (as did the shape of the curves) that

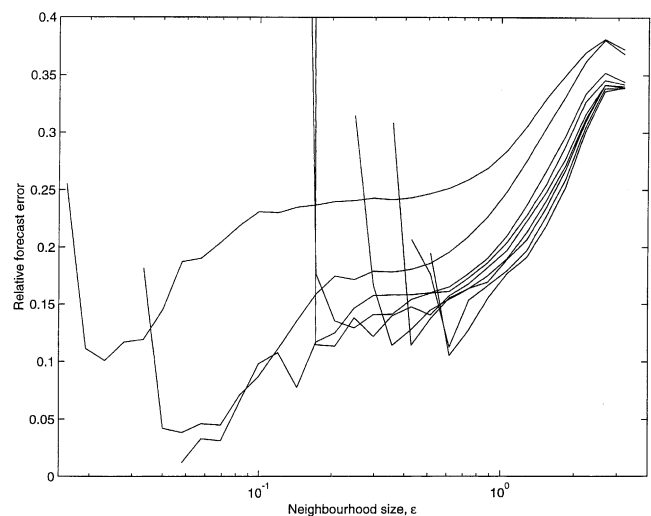


Fig. 8. The DVS plots for p_2 from the lg9 data, time-delay-embedded with $d=3$. The embedding dimension m varied from 2 (top curve) to 10.

there was very little noise in the data. Probably as a result of the relatively large discretization artefact, amounting to noise, the Q_1 curves yielded less information. The curves effectively ceased varying for $m \geq 6$, indicating that this many dimensions were needed for an adequate embedding of the data. By producing similar families of curves for the Rössler attractor subjected to similar amounts of digitisation artefact (limited number of samples per cycle, and of bits of range resolution), we showed that the apparent embedding dimension was increased from 3 to 4 by these effects. On this basis, it can be argued that the embedding dimension indicated for the lg9 system in the absence of these data effects would be 5, still high-dimensional. The increasing prediction error with size at all m in the lg9 data clearly shows nonlinear behaviour. However, while the relatively small range of neighbourhood sizes at which the ability to fit is lost suggests a low noise level, nevertheless the eventual left-hand-side up-swoop of each curve at a point that depends on m does show that there was a source of stochasticity present. Thus the system is presumed by default to be irregular (aperiodic) as a result of nonlinear stochastic rather than nonlinear deterministic processes.

Going beyond the locally linear predictors, we tried to fit a globally nonlinear model to the U-shaped return map of Fig. 4. Since Hegger et al. [20] warn that “polynomials diverge outside the data and hence can be unstable under iteration”, we used Tisean’s radial-basis-function¹ routine, and fits were compared over the range $m=1$ to 6 and $p=6$ to 40, p being the number of radial basis functions, as shown for $p=10$ to 38 in Fig. 9. Calculated out-of-sample prediction error was consistently least at the maximum p but with $m=3$, whereas the corresponding plot by no means seemed the best fit to the input data. By inspection, the model for $m=3$ and $p=18$ was selected for further use. We calculated $S(e, m, t)$ for the data of that map, along with the data of the raw-data return map which inspired it, and the data of the map produced by our polynomial model.

The raw section data were, like the original flow data, linear in S vs. $\ln t$, indicating power-law (stochastic) divergence. The slope was 0.97 with $m=5$, and 1.1 with $m=6$ and 7. Both the radial-basis-function and

polynomial models were far from linear on these axes, but close to linear in S vs. t , as shown in Fig. 10, indicating the expected deterministic behaviour.

5. Discussion and conclusions

The data were shown to be stationary (via recurrence plotting) and to emanate from a nonlinear system (by comparison with surrogates). Application of the false-nearest-neighbours method suggested that an embedding dimension of 3 might suffice, but on the other hand, attempts to find a correlation dimension gave no consistent answer in the range 4–6. Similarly, the outcomes of locally linear prediction, as expressed in the Casdagli DVS plot, suggest that an embedding dimension of at least 6 is needed. There was a hint here, through deliberately creating similar effects in an analytical attractor, that the underlying dimension might be lower were the data not subject to the combined influences of excessive discretization in both time and signal level.

Despite signs also from the radial-basis-function modelling of the U-shaped return map that an embedding dimension of 3 might be sufficient, overall the tests applied to the data tended to show outcomes that varied with embedding dimension up to 6, indicating that the oscillation complexity is ruled by processes which manifest in time-series data as high-dimensional dynamics.

There were signs that the distributed nature of the system was playing a role in this: the clumping of first-return times suggests, as did behaviour seen by Bertram and Sheppard [16], that there are preferred oscillation periods, probably set by wave travel and reflection between the ends of the tube, a phenomenon which is not comprehended in data sets consisting of the variable value vs. time only. Such non-comprehended behaviour would lead time-series data sets to show high-dimensional determinism, since it is essentially a manifestation of the spatially distributed nature of the system. If therefore the system, being fluid-dynamic and ultimately ruled by (infinite-dimensional) partial differential equations, does not confine itself to effectively low-dimensional (ordinary differential equation) behaviour, analysis of time series is doomed to find the result that the dimension is high. This may result from either genuinely high- but finite-dimensional dynamics (as in the Mackey-Glass delay differential equation model of blood generation for leukaemia patients—see Farmer [36]), or distributed effects amounting to infinite-dimensional dynamics, or stochastic influences on a nonlinear deterministic system.

Thus the analyses of the lg8 and lg9 data point to the necessity of analysis of data which reflect the spa-

¹ Radial basis functions were introduced into time series analysis by Broomhead and Lowe [35]. Following Kantz and Schreiber [21], one defines scalar $\Phi(r)$, where r is positive, and the vector positions y_i of the k centres, then $F(\tilde{x}) = \alpha_0 + \sum_{i=1}^k \alpha_i \Phi(\|\tilde{x} - \tilde{y}_i\|)$. Typically Φ is bell-shaped with maximum at $r=0$. If the centres and widths are kept constant, determining the $k+1$ coefficients α_i , $i=0$ to k , is then a linear problem of least-squares fitting. The width can be optimised by testing several values, since the least-squares problem for each is quick to solve. The Lorentzian radial basis function used here is $\Phi = \frac{1}{1+r^2/a^2}$.

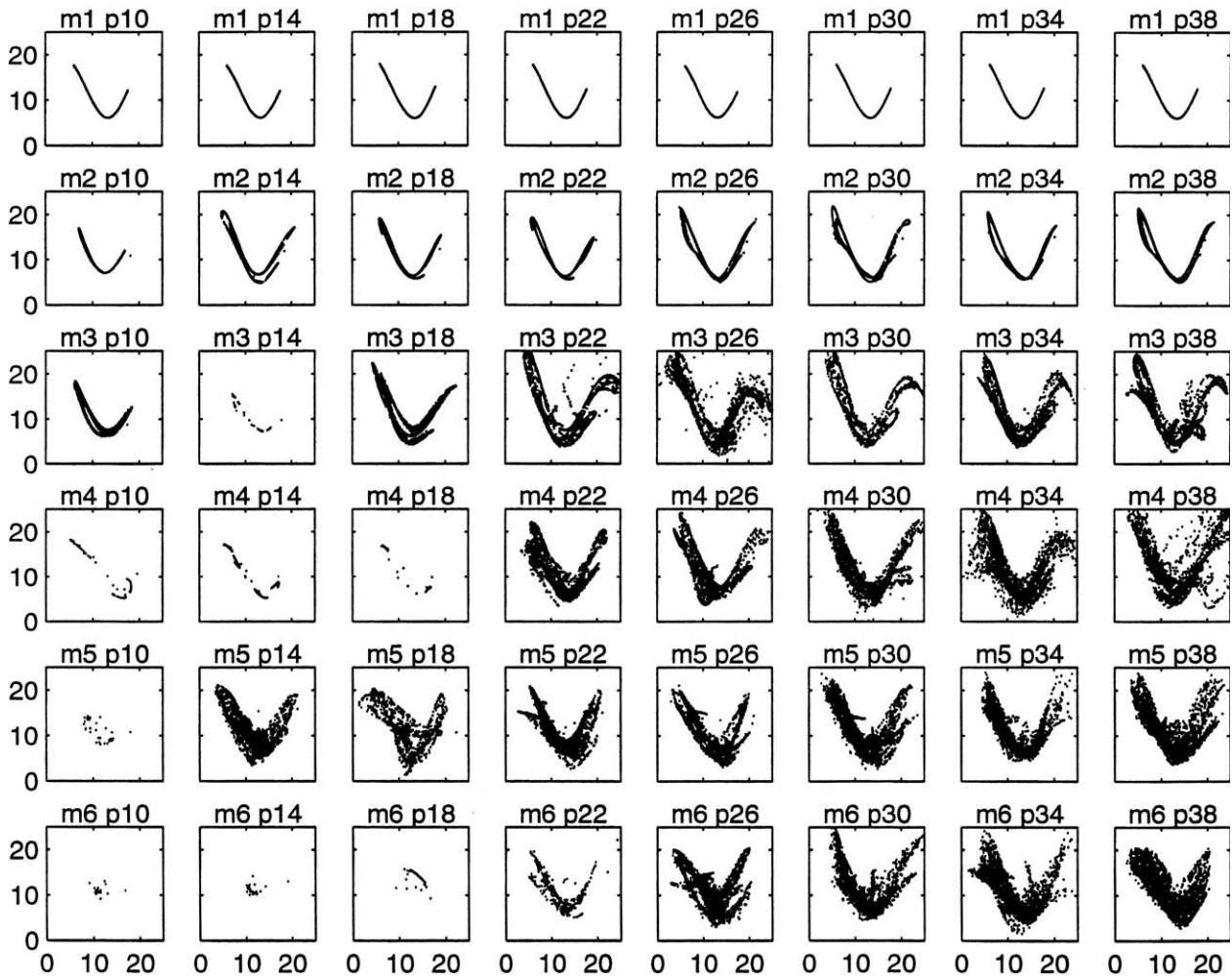


Fig. 9. The first-return maps achieved by radial-basis-function models with $m=1$ to 6 and $p=10$ to 38 fitted to the U-shaped return map of Fig. 4a. Of the 2166 data points, 500 were used to fit the model in each case; the remainder were used to estimate out-of-sample error.

tially distributed nature of the system. Data on the instantaneous variation of internal cross-sectional area and pressure along the length of the oscillating collapsible tube, i.e. $A(x, t)$ and $p(x, t)$, were obtained by Bertram and Godbole [37], but the methodology used necessarily limited the observations to strictly periodic oscillations. One of the initial premises of this investigation was that aperiodic oscillations might contain information on the nature of the system which is absent from fully periodic oscillations, information which could be revealed through application of the tools of nonlinear dynamics. Nevertheless, we considered the possibility of fitting an appropriate distributed model to the $A(x, t)$ and $p(x, t)$ data. We recreated the one-dimensional model of Jensen [7]. The model involves partial differential equation integration by the two-step MacCormack method [38], and is far from robust or straightforward to implement. Jensen originally achieved solutions only by extremely problem-specific modifications to the basic integration

scheme, modifications which we found we had to emulate in detail. The eventual computation proved intensive, even by the improved standards of today's personal computers, to the point where a parameter fit by iteration of the model against the distributed data would have been impractical. We were in any case discouraged from pursuing such a parameter fit by irreconcilable differences between the assumptions underlying the equations of the Jensen model and the circumstances of the experiments reported by Bertram and Godbole; these differences are discussed by Jensen [7] and Bertram et al. [39].

We attach great importance to the result of our investigations of largest Lyapunov exponent. The power-law divergence of initially neighbouring points was interpreted as implying a nonchaotic origin of the stretching. In theory, if this log-log slope is $1/2$, the implication is that the distance growth could be diffusive (Brownian motion), although in an SDE, interaction between the dynamics and the noise can be shown

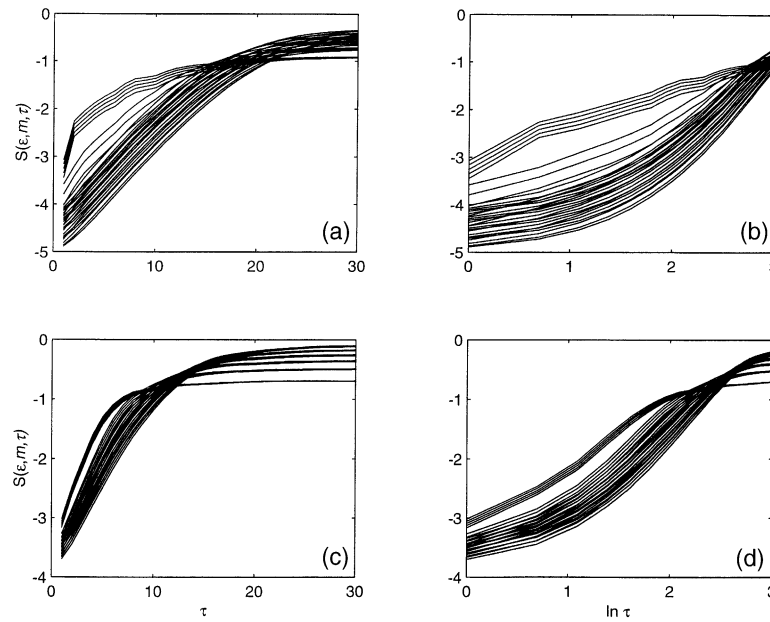


Fig. 10. The plots of S vs. t and S vs. $\ln t$ for the selected radial-basis-function model ($m=3$, $p=18$), and the sixth-order-polynomial nonparametric model, both fitted to the return-map data of Fig. 4. The polynomial model is shown in panels a and b; the radial-basis-function model is shown in panels c and d.

to cause slopes that vary from this value [40]. The non-exponential divergence of near neighbours pointed unambiguously to stochastic, rather than deterministic, nonlinear dynamics. If stochastic influences are partly or wholly responsible for the aperiodicity of the observed oscillations, then the underlying system, like the noise-perturbed Van der Pol oscillator that we proposed as a surrogate, might well be periodic in the absence of the random forcing².

This outcome should be considered along with the shape of the DVS plots. The latter showed conclusively that the data portrayed a nonlinear system. In view of the sigmoidal shape of the tube law relating transmural pressure to cross-sectional area (a relation strictly valid only for an infinitely long tube) for a collapsible tube, this is perhaps unsurprising. Of greater interest was the finding that the ability to predict the future course of the data on small scales was affected by noise, albeit of small amplitude. The data cannot therefore be distinguished from those which could be produced by a good surrogate which was perturbed from periodicity only by such noise. We give an example of a plausible surrogate based on the Van der Pol oscillator, which has itself been proposed in the past as a black-box (nonfluid-mechanically based) model of a collapsible tube. There is thus no basis on which to maintain that the recorded data are a manifestation of chaotic

dynamics. Despite the large number of intriguing behaviours noted herein and in past papers of Bertram and colleagues suggestive of deterministic aperiodicity, it is not necessary to postulate a deterministic mechanism behind the data examined here, and so this unnecessary hypothesis should be rejected.

This conclusion is somewhat surprising, in that the dynamical preconditions for chaotic behaviour are clearly satisfied in a collapsible tube. We cannot say that collapsible tubes are incapable of chaotic dynamics, but we do say that the data on the subject thus far do not verify the notion. The great majority of investigations of collapsible-tube oscillations have found only periodicity; indeed a recent study of a thinner-walled tube in our laboratory, with all conditions similar to those used previously except tube thickness [4], found large numbers of qualitatively distinct periodic oscillation waveforms but no aperiodic oscillation. This is particularly notable in that the prime candidate for the source of stochastic forcing in the thick-walled collapsible tube considered here is the turbulent flow through the tube, at Reynolds numbers around 100 times the flow-rate in ml/s. The flow-rates through the thin-walled tube reached Reynolds numbers in excess of 30,000, but without provoking significant aperiodicity. Since investigations elsewhere have likewise concentrated on relatively thin-walled tubes, and have not found aperiodicity, it must be presumed that thick-walled tubes are pre-disposed to aperiodic behaviour. This may relate to the somewhat higher thresholds of flow-rate and negative transmural pressure that are needed to

² Aperiodicity can also arise in theory through the addition of noninteracting oscillators of incommensurate period, but this is not a realistic model of the physical system here.

induce oscillations in such a tube. It may also relate to the extreme changes in compliance which are found for such a thick-walled silicone-rubber tube as it moves from distension to first buckling and to first opposite-wall contact [41]. In contrast, thinner silicone-rubber tubes, and latex ones, seem to display a more progressive collapse behaviour. This idea is reinforced by consideration of the tapered-thickness tube investigated by Bertram and Chen [42], which at the upstream end had the same thick wall as the uniform tubes in which the aperiodic oscillations were observed. Collapse was progressive at every cross-section of the tapered tube, because of the greater stiffness just upstream, and again only periodic oscillations were observed (excluding modes specific to such tapered tubes).

The other intriguing aspect of the outcomes of this investigation is the extent to which they reinforce the apparent similarity between the experimental fluid-dynamic system and the lumped-parameter model of Bertram and Pedley [15]. In the world of collapsible-tube-flow models, this model is considered thoroughly obsolete relative to the more detailed models that have followed, which have allowed the continuous specification of variables in one, two or even three spatial dimensions. Yet the experimental data available so far seem to follow two important predictions [13,18] stemming from that model: (1) that despite strong non-linearity and at least three degrees of freedom, chaotic oscillation is impossible while the upstream pressure head is steady, and (2) that chaotic behaviour ensues (as it does—see Bertram and She [17]) once the upstream head is itself made pulsatile at a frequency that competes with the natural frequency of self-excited oscillation. The computational difficulty associated with integration forward in time of most if not all of the spatially distributed models has so far inhibited the production of equally forthright predictions for experimental test. We can therefore conclude that this reappraisal of what had earlier seemed to be chaotic oscillation of flow through a collapsible tube with steady driving head brings the experimental and theoretical sides of this subject into a happy correspondence for the time being.

Finally, the outcome of this investigation shows clearly the need for great care in the analysis of aperiodic data. While we are not the first to make this point, the results shown here, taken together with those of Bertram et al. [2] and Bertram [10], demonstrate how a system can exhibit behaviour that predisposes to the assumption of chaos. From there, it is a short step to being all too easily satisfied by the outcomes of inconclusive or ambiguous tests that chaos has indeed been found. In this case the data emanate from an experimental system, but the problem can equally arise in the context of numerical modelling, where it is compounded by the possibility of the physics behind the

model equations being changed artefactually in the numerical realization. We advocate a very high threshold of suspicion, and rigorous testing along the lines reported here, before acceptance of aperiodicity as chaos.

Acknowledgements

CDB was the recipient of a scholarship from the Deutscher Akademischer Austauschdienst (German Academic Exchange Service). We thank Professor Oliver Jensen for assistance in the implementation of his model. The experiments giving rise to the data analysed here were largely funded by the Australian Research Council.

References

- [1] May RM. Simple mathematical models with very complicated dynamics. *Nature* 1976;261:459–67.
- [2] Bertram CD, Raymond CJ, Pedley TJ. Application of dynamical system concepts to the analysis of self-excited oscillations of a collapsible tube conveying a flow. *Journal of Fluids and Structures* 1991;5:391–426.
- [3] Thompson JMT, Stewart HB. *Nonlinear dynamics and chaos*. John Wiley and Sons; 1986.
- [4] Bertram CD, Elliott NSJ. Flow-rate limitation in a uniform thin-walled collapsible tube, with comparison to a uniform thick-walled tube and a tube of tapering thickness. *Journal of Fluids and Structures* 2003;17:541–59.
- [5] Broomhead DS, King GP. Extracting qualitative dynamics from experimental data. *Physica D* 1986;20:217–36.
- [6] Broomhead DS, Jones R, King GP. Topological dimension and local coordinates from time series data. *Journal of Physics A: Mathematical & General* 1987;20:L563–9.
- [7] Jensen OE. Chaotic oscillations in a simple collapsible-tube model. *ASME Journal of Biomechanical Engineering* 1992;114:55–9.
- [8] Cancelli C, Pedley TJ. A separated-flow model for collapsible-tube oscillations. *Journal of Fluid Mechanics* 1985;157:375–404.
- [9] Bertram CD, Tian X. Correlation of local stretchings as a way of characterising chaotic dynamics amid noise. *Physica D* 1992;58:469–81.
- [10] Bertram CD. Dynamical system analyses of aperiodic flow-induced oscillations of a collapsible tube. *Journal de Physique III France* 1995;5:2101–16.
- [11] Wolf A, Swift JB, Swinney HL, Vastano J. Determining Lyapunov exponents from a time series. *Physica D* 1985;16:285–317.
- [12] Smith LA. Quantifying chaos with predictive flow and maps: locating unstable periodic orbits. In: Abraham NB, et al., editors. *Measures of complexity and chaos*. NATO ASI Series. Plenum Press; 1990.
- [13] Armitstead JP, Bertram CD, Jensen OE. A study of the bifurcation behaviour of a model of flow through a collapsible tube. *Bulletin of Mathematical Biology* 1996;58:611–41.
- [14] Doedel E, Wang X. *Auto 94: software for continuation and bifurcation problems in ordinary differential equations*. California Institute of Technology Applied Mathematics Report; 1994.
- [15] Bertram CD, Pedley TJ. A mathematical model of unsteady collapsible tube behaviour. *Journal of Biomechanics* 1982;15:39–50.

- [16] Bertram CD, Sheppard MD. Interactions of pulsatile upstream forcing with flow-induced oscillations of a collapsed tube: mode-locking. *Medical Engineering and Physics* 2000;22:29–37.
- [17] Bertram CD, She J. Chaotic and mode-locked interactions between flow-induced collapsible-tube oscillation and pulsatile upstream forcing. In: Broomhead DS, et al., editors. *Stochastic and chaotic dynamics in the lakes*. Melville, NY, USA: American Institute of Physics; 2000, p. 510–6.
- [18] She J, Bertram CD. Numerical simulation of collapsible-tube flows with sinusoidal forced oscillations. *Bulletin of Mathematical Biology* 1996;58:1023–46.
- [19] Bertram CD, Butcher KSA. A collapsible-tube oscillator is not readily enslaved to an external resonator. *Journal of Fluids and Structures* 1992;6:163–80.
- [20] Hegger R, Kantz H, Schreiber T. Practical implementation of nonlinear time series methods: the TISEAN package. *Chaos* 1999;9:413–35.
- [21] Kantz H, Schreiber T. *Nonlinear time series analysis*. Cambridge University Press; 1997.
- [22] Schreiber T, Schmitz A. Surrogate time series. *Physica D* 2000;142:346–82.
- [23] Takens F. Detecting strange attractors in turbulence. In: Rand DA, Young L-S, editors. *Dynamical Systems and Turbulence* (Warwick, England, 1980), vol. 898 of *Lecture Notes in Mathematics*. Berlin: Springer-Verlag; 1980, p. 366–81.
- [24] Fraser AM, Swinney HL. Independent coordinates for strange attractors from mutual information. *Physical Review A* 1986;33:1134–40.
- [25] Grassberger P, Hegger R, Kantz H, Schaffrath C, Schreiber T. On noise reduction methods for chaotic data. *Chaos* 1993;3:127–141.
- [26] Schroer CG, Sauer T, Ott E, Yorke JA. Predicting chaos most of the time from embeddings with self-intersections. *Physical Review Letters* 1998;80:1410–3.
- [27] Kennel MB, Brown R, Abarbanel HDI. Determining embedding dimension for phase-space reconstruction using a geometrical construction. *Physical Review A* 1992;45:3403–11.
- [28] Grassberger P, Procaccia I. Measuring the strangeness of strange attractors. *Physica D* 1983;9:189–208.
- [29] Casdagli M. Chaos and deterministic versus stochastic non-linear modelling. *Journal of the Royal Statistical Society B* 1992;54:303–28.
- [30] Bertram CD. An adjustable hydrostatic-head source using compressed air. *Journal of Physics E, Scientific Instruments* 1986;19:201–2.
- [31] Voss HU, Schwache A, Kurths J, Mitschke F. Equations of motion from chaotic data: a driven optical fiber ring resonator. *Physics Letters A* 1999;256:47–54.
- [32] Breiman L, Friedman JH. Estimating optimal transformations for multiple regression and correlation. *Journal of the American Statistical Association* 1985;80:580–619.
- [33] So P, Ott E, Sauer T, Gluckman BJ, Grebogi C, Schiff SJ. Extracting unstable periodic orbits from chaotic time series data. *Physical Review E* 1997;55:5398–417.
- [34] Kantz H. A robust method to estimate the maximal Lyapunov exponent of a time series. *Physics Letters A* 1994;185:77–87.
- [35] Broomhead D, Lowe D. Multivariable functional interpolation and adaptive networks. *Complex Systems* 1988;2:321–55.
- [36] Farmer JD. Chaotic attractors of an infinite-dimensional dynamical system. *Physica D* 1982;4:366–93.
- [37] Bertram CD, Godbole SA. Area and pressure profiles for collapsible tube oscillations of three types. *Journal of Fluids and Structures* 1995;9:257–77.
- [38] Roache PJ. *Computational fluid dynamics*. Albuquerque, New Mexico: Hermosa Publishers; 1972.
- [39] Bertram CD, Sheppard MD, Jensen OE. Prediction and measurement of the area-distance profile of collapsed tubes during self-excited oscillation. *Journal of Fluids and Structures* 1994;8:637–60.
- [40] Timmer J, Häußler S, Lauk M, Lücking CH. Pathological tremors: deterministic chaos or nonlinear stochastic oscillators?. *Chaos* 2000;10:278–88.
- [41] Bertram CD. The effects of wall thickness, axial strain and end proximity on the pressure-area relation of collapsible tubes. *Journal of Biomechanics* 1987;20:863–76.
- [42] Bertram CD, Chen W. Aqueous flow limitation in a tapered-stiffness collapsible tube. *Journal of Fluids and Structures* 2000;14:1195–214.